

# Mechanistic insight into deep holes from interband transitions in Palladium nanoparticle photocatalysts

Pin Lyu<sup>1</sup>, Randy Espinoza<sup>1</sup>, Md. Imran Khan<sup>2</sup>, William C. Spaller,<sup>1</sup> Sayantani Ghosh<sup>2</sup>, and Son C. Nguyen<sup>1,\*</sup>

<sup>1</sup> Department of Chemistry and Chemical Biology, University of California Merced, 5200 North Lake Road, Merced, California 95343, United States

<sup>2</sup> Department of Physics, University of California Merced, 5200 North Lake Road, Merced, California 95344, United States

\* Email: [son@ucmerced.edu](mailto:son@ucmerced.edu)

## Abstract

Photocatalysis of metallic nanoparticles, especially utilizing hot electrons generated from localized surface plasmon resonance, is of widespread interest. However, the role of hot holes, especially generated from interband transitions, has not been emphasized in exploring the photocatalytic mechanism yet. In this study, a photocatalyzed Suzuki-Miyaura reaction using mesoporous Pd nanoparticle photocatalyst served as a model reaction to study the role of hot holes by accurately measuring the quantum yields of the photocatalyst. The quantum yields increase under shorter wavelength excitations and correlate to the “deeper” energy of the holes from the Fermi level. Our mechanistic study suggests that deeper holes in the *d*-band can catalyze the oxidative addition of aryl halide R-X onto Pd<sup>0</sup> at the surface of nanoparticles to form the R-Pd<sup>II</sup>-X complex, the rate-determining step of the established catalytic cycle. We pointed out that this deep hole mechanism should deserve as much attention as the well-known hot electron transfer mechanism in previous studies.

## Introduction

Metallic nanoparticles have gained a growing interest for applications in photocatalysis.<sup>1-17</sup> The strong light absorption, high surface-area-to-volume ratio, and robust nature of these nanoparticles make them great potential candidates for exploring better photocatalytic activities and high recyclability. Historically, photocatalysis induced by localized surface plasmon resonance (plasmon resonance for short) of these particles has been studied widely for more than a decade,<sup>15,16,18-21</sup> but photocatalysis originating from interband excitations is still underexplored.<sup>7,10,12,22,23</sup> In short, the plasmon resonance can be described by a classical picture as a collective oscillation of the nanoparticles’ electrons in response to electric field of exciting photons or a quantum mechanical picture as electron transitions from some *sp*-band states to other *sp*-band states (*i.e.* intraband transitions), while the interband transitions are given to electron transitions from the respective *d* to *sp* bands. Due to these origins, the plasmon resonance of metal nanoparticles offers strong optical absorption and tunable spectral shift depending on the particle morphology, but the interband transitions always provide a significant absorption within a defined spectral region. The optical excitations in these two regimes are expected to exhibit different catalytic outcomes because the generated hot carriers have different energy states, population and dynamics for each regime.<sup>24-26</sup> With the generation of hot electrons above the Fermi level ( $E_F$ ) and hot holes near  $E_F$  by the plasmon resonance, the extraction of the hot electrons is more favorable than that of the hot holes, and electron transfer from the nanoparticle photocatalysts to reactants (reductive pathway) is generally preferred. This catalytic mechanism has been demonstrated in many reductive reactions, such as reduction of CO<sub>2</sub> or nitro compounds.<sup>15,17</sup> Recently, the hot holes

could also be utilized for some oxidative reactions, such as alcohol oxidation.<sup>27-30</sup> On the other hand, interband transitions, generating “deeper” holes below  $E_F$  and electrons near  $E_F$ , are more suitable for the oxidative pathway where the nanoparticle photocatalysts are better used for hole-mediated oxidation reactions. This suggested mechanism will provide a new perspective in understanding the photocatalysis of metal nanoparticles and designing better photocatalyzed reactions.

In order to shed light on the catalytic mechanisms in previous experiments, many research groups have compared the catalytic efficiencies under these two excitations, but it has been difficult to disentangle the origin of the observed efficiencies due to the strong spectral overlap of these two excitations.<sup>10,16,31-33</sup> For example, the plasmon resonance of spherical gold nanoparticle catalysts in the region around 480 to 650 nm is spectrally overlapped with the intrinsic *d-to-sp* interband transitions. These interband transitions have strong absorption in the ultraviolet region and extend to the visible region with an absorption tailed up to about 600 nm.<sup>34</sup> Thus it is desirable to tune the plasmon resonance absorption away from the interband absorption to resolve the catalytic mechanism. This approach is demonstrated in this paper by using mesoporous structure.

In this study, mesoporous Pd nanoparticles were employed due to their spectral shift of plasmon resonance from visible to near-infrared regions and the dominant contribution of interband transitions in the optical region that we surveyed (*i.e.*, 400-600 nm). Usually, the non-porous Pd nanoparticles have a plasmon resonance associated with a very broad spectral feature in the ultraviolet-visible region, and this plasmonic peak appears on top of the entire spectral region of the interband transitions (Fig. 1a).<sup>35,36</sup> In contrast, the porous version shows a featureless absorption with no peak of plasmon resonance in the 400-600 nm region (Fig. 1a), therefore the observed photocatalytic activities could be attributed mainly to interband transitions. Another advantage of the mesoporous structure is the shorter travel distance for hot carriers diffusing to particles' surface, thus the efficiency of harvesting them is expected to be improved.<sup>11</sup>

The Suzuki-Miyaura reaction between bromobenzene and phenylboronic acid in water was used as a prototype reaction to evaluate the catalytic activities induced by interband transitions of porous Pd nanoparticles. Generally, the rate-determining step of this reaction is the oxidative addition of the aryl halide, which was proposed to be accelerated by hot electrons generated from the photocatalysts.<sup>15,37,38</sup> The performance of these photocatalysts was evaluated by their quantum yields; monitoring the quantum yields under photoirradiation at different wavelengths provided more mechanistic insight. As demonstrated in this work, keeping the same photon flux and reaction time (besides of preparing the same chemical concentration and temperature) was a critical experimental condition to make a fair comparison of the quantum yields across different excitation wavelengths. It was found that leaching of Pd from the mesoporous Pd nanoparticles was not a major contribution to the observed catalytic activities. Eventually, the observed wavelength dependence of quantum yields was correlated with the wavelength dependence of the energy state of hot carriers, and a possible mechanism was proposed. This mechanism was overlooked in some previous studies<sup>38-41</sup>, and it deserves more attention in utilizing hot carriers for catalysis.

## Results

### Optical property and photocatalyzed condition of mesoporous Pd nanoparticles

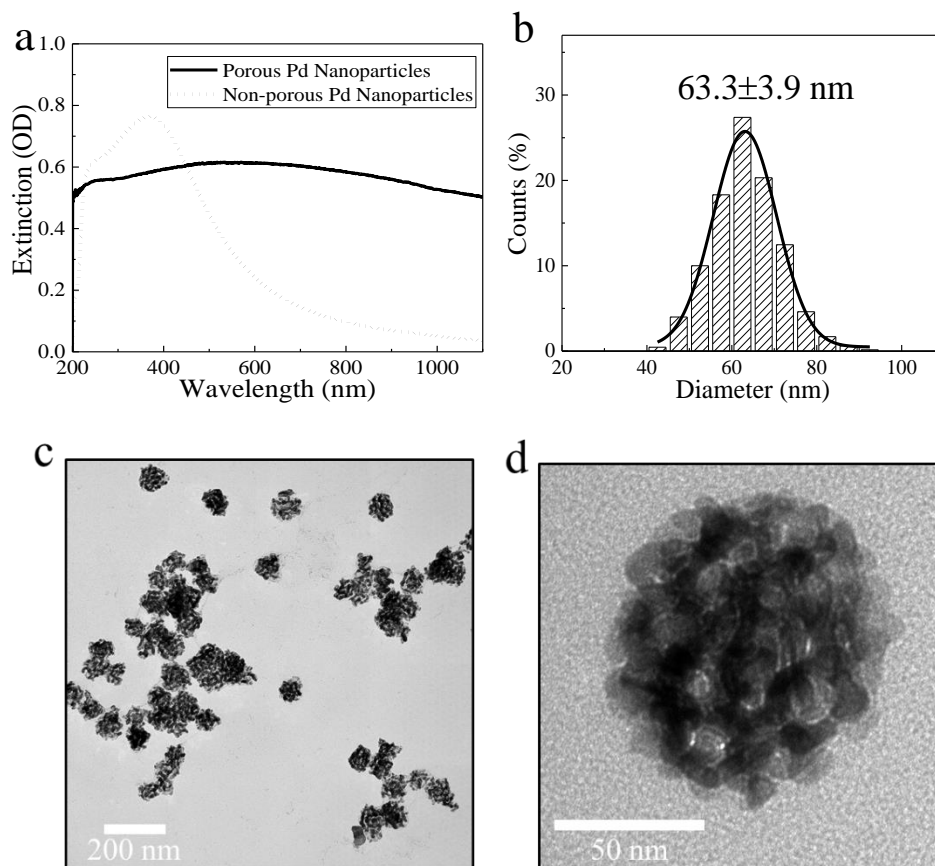


**Fig. 1 Optical and morphological characterization of mesoporous Pd nanoparticles.** (a) UV-Vis spectra of colloidal mesoporous Pd nanoparticles (solid line) in water and non-porous 50 nm Pd nanoparticles solution (dotted line) for comparison. (b) Size distribution based on analyzing 500 nanoparticles from SEM image in Supplementary Fig. 3a. (c, d) Representative TEM images of mesoporous Pd nanoparticles.

Mesoporous Pd nanoparticles were prepared by a typical hard-template wet-chemical method, in which polystyrene-block-poly(ethylene oxide) and ascorbic acid acted as the template and the reductant, respectively.<sup>42</sup> The as-synthesized particles were cleaned by tetrahydrofuran (THF) and calcinated at 200 °C for one hour to remove the solvent and most of the polymer, and the porous structure was still preserved.<sup>42</sup> The dry particles were further characterized and used as the catalyst. Fourier-transform infrared spectroscopy (FTIR) did not detect any vibrational signal of organic compounds on the dry particles, indicating that the catalyst does not have much polymer left (Supplementary Fig. 1). Thermogravimetric analysis (TGA) confirmed that 22 % of the dry particles' weight is the leftover polymer (Supplementary Fig. 2). The particles have an average hydrodynamic diameter of  $79.9 \pm 5.9$  nm and a zeta potential of 0.6 mV when dispersed in water and measured by dynamic light scattering (DLS), a narrow size distribution of  $63.3 \pm 3.9$  nm as determined by scanning electron microscopy (SEM) (Fig. 1b and Supplementary Fig. 3a), and an average pore size of  $11.3 \pm 3.3$  nm (analyzed 100 pores in Fig. 1c). The porous Pd nanoparticles had a large specific Brunauer, Emmett and Teller (BET) surface area of  $57.1 \text{ m}^2/\text{g}$  and average pore size of 5.6 nm, determined by  $\text{N}_2$  adsorption-desorption isotherms (See details in

Supplementary Fig. 4). The particles have polycrystalline structures with grain sizes that are larger than the pore wall thickness<sup>42</sup>, and the pores form open channels throughout the particles as shown in a series of tilt transmission electron microscopy (TEM) images (Supplementary Fig. 5).

The mesoporous Pd nanoparticle solution has a broad UV-Vis spectrum as compared to that of non-porous forms (Fig. 1a).<sup>35,36</sup> For example, the non-porous 50 nm Pd nanoparticles (see a SEM image in Supplementary Fig. 3b) with a comparable mass to our catalyst have a broad absorption peak at 370 nm due to both plasmon resonance and interband transitions, but the absorption drops significantly in the red-photon and longer wavelength regions.<sup>36,43</sup> In contrast, the porous particles' plasmon resonance absorption shifted significantly to these low energy regions (Fig. 1a). Similarly, the mesoporous form of gold or platinum nanoparticles also shows significant red-shifts of plasmon resonances to the near IR regions.<sup>44,45</sup> The plasmonic coupling between adjacent crystal domains or pore walls within proximity may be responsible for these red-shifts.<sup>42,46</sup> On a drop-cast sample, the scattering intensity measured by an integrating sphere and a tunable laser follows approximately a  $1/\lambda^4$  dependence, resembling Rayleigh scattering (Supplementary Fig. 6). Further measurement by a home-built setup for determining optical scattering and extinction on the colloidal solution in a 1x1cm quartz cuvette showed that the total light scattering in the range of 400 to 800 nm of the colloidal solution was almost neglectable. This result indicated that less than 3 % of the incident photons were scattered from the photocatalyst and more than 97 % were absorbed (Supplementary Fig. 7 and Supplementary Note 1). From these results, it was concluded that the porous Pd nanoparticles had strong absorbance in the 400-600 nm region, and the dominant contribution to this absorbance is the interband transitions.

Suzuki–Miyaura reactions have been employed to evaluate the photocatalytic performance of Au–Pd alloy nanoparticles or Pd nanoparticles loaded on metal oxides or WS<sub>2</sub>.<sup>38,47-49</sup> Besides the versatile applications of this reaction in creating C-C bonds and the transparent solutions of reactants and products for convenient photocatalysis study, the oxidative addition of aryl halides (*i.e.*, the rate-determining step of the catalytic cycle)<sup>50</sup> could be catalyzed by hot electrons generated from photo-exciting the Pd nanoparticle catalyst. In our typical reaction condition at room temperature with different light-emitting diode (LED) light sources, bromobenzene and phenylboronic acid served as the coupling partners, sodium hydroxide as a base, and cetyltrimethylammonium chloride (CTAC) as a solubilizer to facilitate the dissolution of organic reactant and product into the aqueous solution (Fig. 2a).<sup>47,48</sup> The zeta potential of the porous Pd nanoparticle photocatalyst is around 60 mV in the reaction solution, which suggests some degree of adsorption of CTAC on the particles and explains for their high stability during the reaction. The biphenyl product was extracted from the reaction solution by dichloromethane and analyzed by proton nuclear magnetic resonance (<sup>1</sup>H-NMR). The reaction time was purposely kept short enough to get a reasonable conversion range for reliable kinetic comparison<sup>51</sup>, though a higher conversion was achieved with a longer reaction time.

The photothermal effect on the catalysis is neglectable in our experiment as local heating is minimal under continuous-wave irradiation and stirring (see detailed explanation in Supplementary Note 2).<sup>52,53</sup> When considering the following processes after a colloidal metal nanoparticle in a stirring solution absorbs a single photon: i) electron thermalization due to electron-electron and electron-phonon couplings (within few picoseconds<sup>54,55</sup>), ii) heat transfer from the particle to the local solvent (within 3 nanoseconds<sup>52</sup>), iii) time gap for absorbing the second photon (about hundreds of nanoseconds, see Supplementary Note 2), then it is obvious that the nanoparticle dissipates all the heat to the surrounding environment long before it absorbs the second photon. Since the hot carriers are well thermalized before the nanoparticle can transfer heat

to the environment, it is reasonable to estimate the average temperature rise of the particle based on the energy of an absorbed photon, specific heat of Pd and the particle's mass. This temperature rise is about 0.001°C under our experimental condition (Supplementary Note 2), which should have no photothermal effect on our studied reaction. Under the constant stirring at high speed of the reaction solution, the transient heat in the LED beam path should be distributed evenly in the entire solution.<sup>56</sup> The macroscopic temperature of reaction solutions rose only 1-2 °C as cooling fans were used. A UV-Vis spectrum of reaction solution without the catalyst showed no obvious absorption at any wavelengths longer than 400 nm (Supplementary Fig. 8a). Blank tests on the reaction without the catalyst under different excitation wavelengths did not show any detectable product yield (Supplementary Table 1). These control experiments confirmed that the light absorption of reactants could be ignored in our experiments, and the reaction under irradiation almost does not happen without the photocatalyst. It is worth noting that the reaction with the catalyst under the dark condition in 6 hours gave a background product yield of 5 %. This background yield was subtracted from the product yields that were used to calculate quantum yields for the photocatalyzed reactions with 6-hour irradiation. For photocatalyzed reactions with shorter irradiation times, the corresponding background yields were extrapolated from the ratios between the actual reaction times and 6 hours. This extrapolation is reasonable for a very low conversion range where the reaction rate is assumed to be unchanged.<sup>57</sup>

### Establishing the same reaction time and photon flux for comparing of quantum yields of photocatalyst under various excitation wavelengths

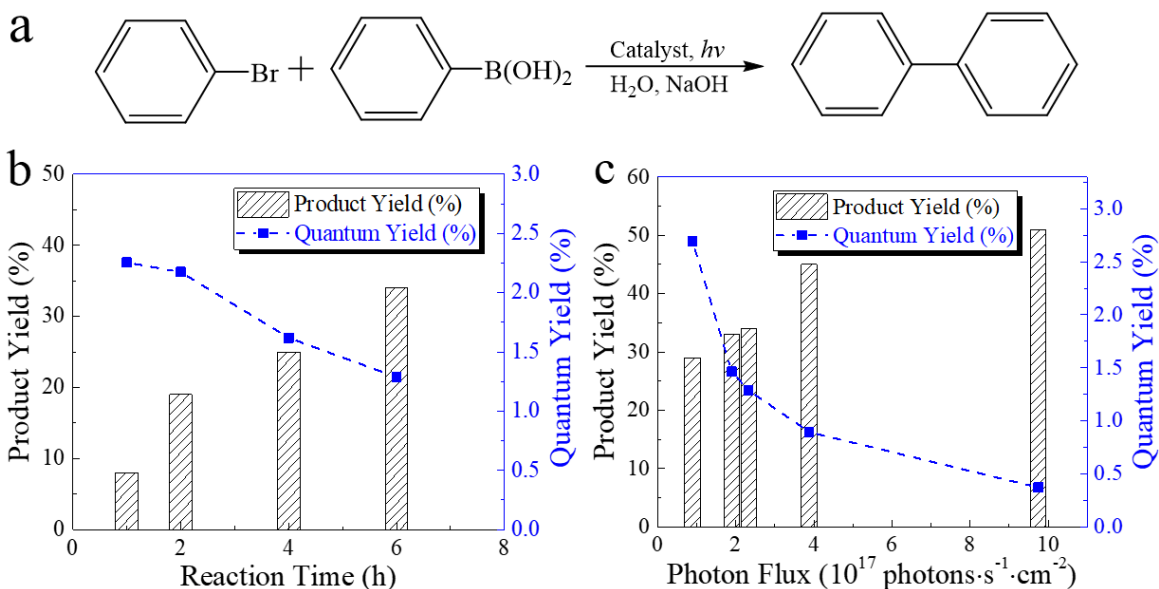


**Fig. 2 Suzuki–Miyaura C-C coupling reaction for evaluating photocatalytic performance of porous Pd nanoparticles.** (a) Typical reaction process and (b and c) Measured product yields (left axis) and quantum yields of the catalyst (right axis) under 405 nm LED irradiation with: (b) different reaction times under the same photon flux (around  $2.4 \times 10^{17}$  photons·s<sup>-1</sup>·cm<sup>-2</sup>), and (c) different photon fluxes under the same 6-hour reaction. Small background product yields of the non-irradiated reactions with the catalyst were subtracted from the observed product yields when calculating the quantum yields.

Quantifying the efficiency of photocatalysts is an important criterion for practical application. This efficiency, here defined as the quantum yield of the catalyst, is calculated as the ratio of the number of product molecules to the number of absorbed photons. This quantity has two important benefits: it helps us understand the photocatalysis mechanism, and it establishes the effective cost of using photons for catalyzed chemical reactions. In practice, when monitoring a photocatalyzed reaction, the quantum yield of the photocatalyst is calculated as the number of product molecules produced per a specific time divided by the number of photons absorbed during that time. These two quantities can be extracted from the measured reaction rate and optical power absorbed by the photocatalyst. It is obvious that the reaction rate decreases as the reaction proceeds. Since the photon absorption rate is unchanged at any given time, the measured quantum yield, as defined above, is expected to be lower when the reaction happens for a longer time. To demonstrate this reasoning, the interval reaction rates were measured (*i.e.*, total product molecules formed/total reaction time in seconds) when the reaction times were varied from 1 to 6 hours under the same absorbed photon flux of a 405 nm LED. The quantum yields reduced from 2.3 % to 1.3 % (Fig. 2b). The same trend was also observed under 490 nm LED irradiation (Supplementary Table 2). This time-dependent behavior is similar to the case of using turn over frequency (TOF) to quantify the efficiency of catalysts under non-irradiated conditions. The measured TOF value always reduces as the catalyzed reaction proceeds, regardless of using homogeneous or heterogeneous catalysts.<sup>57,58</sup> The TOF does not entirely reflect the kinetics of a catalyzed reaction, and the rate law should be the better description.<sup>58</sup> In our study, since we wanted to compare quantum yields of the photocatalyst under various excitation wavelengths, we did not need to derive a rate law of our photocatalyzed reaction under each excitation wavelength. However, we did need to have the photocatalyzed reactions run for the same time interval when comparing quantum yields of the catalyst under different excitations.

Using a similar argument based on chemical kinetics as mentioned above, a higher photon flux condition creates more photo-excited nanoparticles, and effectively causes higher product yield and lower reactant concentration. As the reaction proceeds, each nanoparticle catalyst encounters a decreasing concentration of reactants, and the efficiency of extracting hot carriers is reduced, hence the quantum yield will be effectively reduced. Using the same reaction condition with 405 nm LED irradiation and 6 hour reaction time for comparison, when the photon flux increases from  $0.9 \times 10^{17}$  to  $9.8 \times 10^{17}$  photons $\cdot$ s $^{-1}$  $\cdot$ cm $^{-2}$ , the measured quantum yield decreases from 2.7 % to 0.4 % (Fig. 2c). A similar trend was observed with 470 nm LED irradiation (Supplementary Table 3). To recap, when comparing the quantum yields of the photocatalyst under different irradiation condition, we should keep not only the same starting experimental condition but also the exact same reaction time and photon flux. This prerequisite is critical for revealing the photocatalytic mechanism in the next section.

## **Wavelength dependence of photocatalytic activities and the proposed catalytic mechanism**

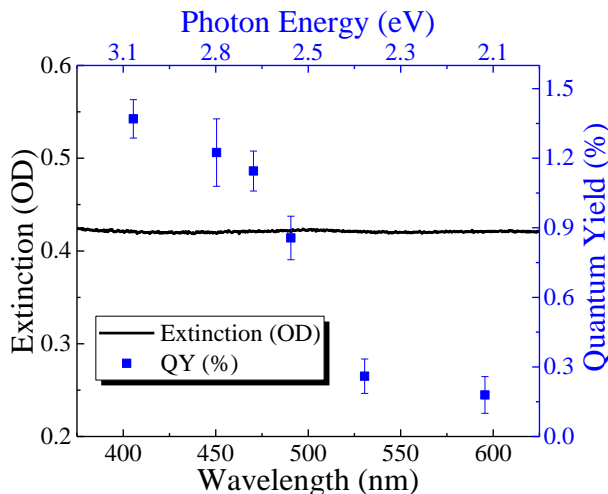


**Fig. 3 Photocatalysis of porous Pd nanoparticles for Suzuki–Miyaura C-C coupling reaction.** Wavelength dependence of quantum yields (right axis) and the optical spectrum of reaction solution with porous Pd nanoparticles (left axis) for comparison. Each error bar is one standard deviation of the mean.

Before moving into the comparison of quantum yields at different excitation wavelengths, we want to examine any catalytic mechanism other than the hot carriers induced photocatalysis mechanism. It is known that leaching of Pd atoms from nanostructures into the reaction solution may complicate the catalytic mechanism<sup>38, 51,59,60</sup>. In our hot filtration tests (see details in Supplementary Note 3), the photocatalyzed reactions were allowed to proceed for one hour followed by the removal of nanoparticles from the reaction solution via centrifugation, then the reactions were allowed to continue for another 5 hours before determining the product yields. These product yields were much lower than those of full reactions with 6-hour irradiation (Supplementary Table 5) but were higher than the yields of control experiments in which the photocatalyzed reactions were only let to react for one hour and the product yield was determined immediately. UV-Vis spectra of the supernatants after 1 h reaction (Supplementary Fig. 9) did not exhibit any noticeable features of  $[\text{PdCl}_4]^{2-}$  complex (Supplementary Fig. 8b) or the mesoporous Pd nanoparticles. These results indicate that the supernatants from hot filtration have little leached Pd that can also catalyze the reaction, and the contribution of leached Pd to the observed catalysis is small. Also, the above result is also consistent with other studies under similar reaction conditions using Au–Pd alloy nanoparticle photocatalyst loaded on  $\text{ZrO}_2$ .<sup>38,61</sup> More importantly, this contribution did not exhibit a clear wavelength dependence in our experiments (Supplementary Table 5). Furthermore, inductively coupled plasma optical emission spectroscopic (ICP-OES) analysis for Pd in the supernatants of the 6-hour reactions under either dark or irradiation conditions showed that the amount of Pd was under detection limit, thus the utmost Pd leached based on the detection limit was estimated to be about 1.2 % of the total Pd in the nanoparticle photocatalyst (See details in Supplementary Note 4). While the chemical structure or formula of this leached Pd species is still unknown and not the focus of this study, another control reaction using  $\text{PdCl}_2$  as the pre-catalyst (the source of generating Pd(0) for the catalytic cycle) showed no wavelength dependence of the product yields (Supplementary Fig. 10). This test indicates that the complete catalytic cycle of the molecular Pd catalyst does not depend on any

tested wavelengths. Lastly, X-ray photoelectron spectroscopy (XPS) showed no distinct changes of the oxidation state of Pd(0) in porous Pd nanoparticles before and after reactions in the dark and photocatalyzed conditions (Supplementary Note 5). Overall, it is clear that the photo-excited Pd nanoparticles, hence the hot electrons and holes generated in the particles, are the key catalysts of the studied reaction, and the wavelength dependence of quantum yields must be attributed to the different states of hot carriers generated by different excitation wavelengths.

In experiments determining the wavelength dependence of quantum yields of the catalyst, the same absorbed photon flux (around  $2.4 \times 10^{17}$  photons $\cdot$ s $^{-1}$  $\cdot$ cm $^{-2}$ ) and reaction time (6 hours) were maintained for each excitation wavelength. Interestingly, the quantum yields do not track the extinction spectrum of porous Pd nanoparticles (Fig. 3). Indeed, the quantum yields are much higher in the shorter wavelength region. In order to explain this observation, it is important to correlate this wavelength-dependent trend with the state of hot holes and electrons generated in the porous Pd nanoparticles at different excitation wavelengths. It is known that each interband transition in *d*-block metals generates a pair of hot electron and hole, in which the hot electron resides near the Fermi level, and the hot hole resides in the *d*-band. When shorter wavelength photons are absorbed, the holes reside at much lower energy states or “deeper” in the *d*-band, but the electrons remain almost the same energy just above the Fermi level.<sup>14,26,62</sup> Thus, a possible photocatalytic mechanism was proposed in Fig. 4, emphasizing on the role of deeper hot holes with stronger oxidizing power for accelerating the oxidative addition step of aryl halide, a rate determining step in the C-C coupling catalytic cycle.<sup>50</sup> In other words, deeper holes have much lower energy than Fermi level, and the lowest possible energy (as compared to vacuum level) is  $E_{hole}^{NP} (eV) = E_F^{NP} - hv$ . The reduction potential of Pd(II)/Pd(0) for the nanoparticle photocatalyst under the influence of these holes,  $E_{Pd(II)/Pd(0)}^{NP-hole}$  (V vs SHE), can be determined by this relationship:  $E_{hole}^{NP} = -4.44 eV + eE_{Pd(II)/Pd(0)}^{NP-hole}$ .<sup>53,63</sup> Thus, deeper holes lower the reduction potential of Pd(II)/Pd(0) and favor the oxidation of Pd on the nanoparticle catalyst. Thus, more R-Pd<sup>II</sup>-X intermediates are produced, and eventually the reaction yields and the quantum yields increase. Fig. 3 shows that the quantum yield starts to pick up at around 530 nm region and increases drastically around 490 nm region, resembling a step-function-like dependence of the quantum yields to the excitation wavelengths. This behavior suggests a threshold of photon energy is needed to overcome the barrier of the oxidative addition reaction.

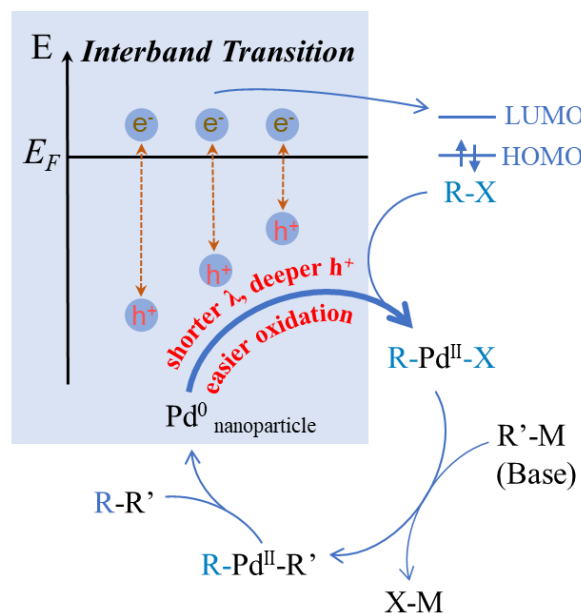


**Fig. 4 Proposed mechanism.** Proposed photocatalytic mechanism of hot holes in accelerating the oxidative addition, a rate-determining step of the catalytic cycle.

The crucial role of hot holes involved in the oxidative addition step was further confirmed by adding a hole scavenger, isopropanol, to the reaction. Under different excitation wavelengths, the product yields were quite close to that of a non-irradiated reaction (Supplementary Table 6). This result can be explained by the fact that isopropanol is a stronger reducing agent ( $E^{\circ}$  of acetone/isopropanol is around 0.76 V vs SHE)<sup>64</sup> than Pd ( $E^{\circ}$  of Pd(II)/Pd(0) is around 0.92 V vs SHE)<sup>65</sup> and that the holes are quenched by isopropanol before they can catalyze the formation of R-Pd<sup>II</sup>-X intermediate. To address the concern of homocoupling of phenylboronic acid<sup>66</sup> that could be catalyzed by the hot holes<sup>15</sup> or bromobenzene to the biphenyl, a series of control experiments using only either reactant showed non-detected product under various irradiation conditions (Supplementary Table 7). Other control experiments with 4-bromoanisole and phenylboronic acid under the dark and 405 nm irradiation conditions confirmed that hetero-coupled 4-methoxy-1,1'-biphenyl was the only product (see details in Supplementary Note 6). In addition, some other possible side reactions including deborylation, debromination or, substitution by hydroxyl group of the reactants were neglectable as compared to the formation of the biphenyl product as confirmed by gas chromatography–mass spectrometry (GC-MS, see details in Supplementary Note 7). Moreover, as we mentioned in our hot filtration tests, the leaching of Pd atoms (in the form of molecular Pd species) has a very small contribution to the observed product yield, thus the R-Pd<sup>II</sup>-X intermediate catalyzed by hot holes is likely to stay on the nanoparticle surface, and the consequent catalytic steps (*e.g.*, transmetalation, reductive elimination) may happen on this surface, as suggested by other studies.<sup>50,67</sup>

Our proposed mechanism provides another insight into the role of deep holes in the photocatalysis of Pd nanoparticles. A previous work using non-porous Pd nanoparticles on ZrO<sub>2</sub> powder concluded that hot electrons played a decisive role in the oxidative addition step. It was proposed that the shorter excitation wavelengths generated higher energy electrons due to interband transitions, and the hotter electrons catalyzed the oxidative addition step better.<sup>48</sup> In fact, as we discussed above, the general physical picture of shorter wavelength excitation in the

interband transition regime is the hot electrons reside near the Fermi level, and hot holes reside deeper in the *d*-band.<sup>14,26,62</sup> Thus, the observed wavelength dependence of the quantum yields in that experiment could be explained by the stronger oxidizing power of the hot holes in the deeper *d*-band, as suggested in Fig. 4. The hot electrons near the Fermi level may activate the aryl halide by promoting electron transfer from the metal to the LUMO of the aryl halide, but this step should not show a strong wavelength dependence in the interband transition regime.

## Discussion

The wavelength dependence of quantum yield or reaction yield of similar C-C coupling reactions was also observed in other photocatalysts,<sup>15</sup> such as Au-Pd alloy nanoparticles supported on ZrO<sub>2</sub><sup>38</sup> or Pd nanoparticles decorated on gold nanorods<sup>47</sup>. However, the role of hot holes generated from interband transitions was not fully explored yet. It is important to mention that our porous Pd nanoparticle photocatalyst has several advantages of revealing the photocatalytic mechanism, such as the suppression of plasmon resonance and the dominant contribution of interband transitions in the optical region studied, a very low light scattering for determining quantum yield with high accuracy, and no interference of supporting materials to the photocatalytic interpretation. Furthermore, our catalyst does show a higher photocatalytic efficiency as compared to the non-porous Pd nanoparticles and some other catalysts under similar experimental conditions (see comparison in Supplementary Table 8), probably because the porous structure increases the probability of hot carrier diffusion to the catalyst's surface.<sup>11,68,69</sup> It is known that the hot holes have smaller kinetic energy and shorter mean free path than electrons do,<sup>26</sup> thus the porous structure may overcome these obstacles.

In summary, the interband transitions of porous Pd nanoparticles were examined to reveal the wavelength-dependent quantum yields of a prototype C-C coupling reaction. With shorter excitation wavelengths, the deeper holes in the *d*-band with stronger oxidizing power can catalyze the oxidative addition of aryl halide R-X onto Pd<sup>0</sup> better to form more R-Pd<sup>II</sup>-X intermediates in the catalytic cycle, thus the quantum yield of the catalyst increases. It is known that the oxidative addition process can be catalyzed by hot electrons, especially electrons with high kinetic energy generated from plasmon resonance.<sup>38,47,48</sup> However, we showed here that interband transitions could also catalyze the oxidation reaction by another process: the strong oxidizing holes can also promote the oxidation of Pd<sup>0</sup> to Pd<sup>II</sup>. We hope this work will prompt more interest in utilizing deep holes from interband transitions for higher photocatalytic efficiency, which has recently picked up some attention.<sup>13,16,70,71</sup>

## Methods

### Synthesis of porous Pd nanoparticles

Mesoporous Pd nanoparticles were synthesized by following the method from the Yamauchi's group. In a 7-mL glass vial, 200  $\mu$ L THF (containing 8 mg PS<sub>(5000)</sub>-b-PEO<sub>(2200)</sub>, Polymer Source Co.), 160  $\mu$ L HCl (2 M), 500  $\mu$ L H<sub>2</sub>PdCl<sub>4</sub> (76.8 mM), 1140  $\mu$ L H<sub>2</sub>O and 2000  $\mu$ L ascorbic acid (0.1 M) were added and under stirring. The glass vial was then put in a water bath set at 50 °C for 10 h reduction reaction to form a dark grey solution, followed by centrifuging at 14,100 g-force and washing with THF and water (3:1 volume ratio) for three times. Eventually, the final product was calcinated in a muffle furnace at 200 °C for one hour to remove the solvent and most of the polymer.

### Characterizations

The mesoporous Pd nanoparticle photocatalyst was characterized by UV-Vis spectroscopy (USB4000, Ocean Optics), DLS (Zetasizer Pro, Malvern Panalytical), SEM (Quanta 200, 5.0 kV, FEI), TEM (Talos F200C G2, 200 kV, Thermo Fisher Scientific), FTIR spectroscopy (Nicolet iS50R, Thermo Fisher Scientific) and TGA (TA Q2000, argon flow at 100 mL/min, heating rate of 10 °C/min, TA Instruments). The biphenyl product was extracted from the reaction solution by dichloromethane, then the solvent was evaporated, and the product was dissolved in deuterated chloroform (CDCl<sub>3</sub>) and quantified by <sup>1</sup>H-NMR (Varian-INOVA 400 MHz, Agilent Technologies) with mesitylene used as the internal standard. There was no signal of any other side products. The amount of leached Pd was determined by ICP-OES (Optima 5300 DV Inductively Coupled Plasma Optical Emission Spectrometer, PerkinElmer). The analyzed samples were prepared by collecting the supernatants after centrifuging the reaction solutions, followed by 800 °C calcination to remove all the organics, digestion with aqua regia, dilution to a final 1-5 % HNO<sub>3</sub> v/v concentration solution, and filtration with 0.2 μm filter. Standard solutions were prepared with trace-metal-free nitric acid from a commercial standard solution (ICP Precious Metal Std, Inorganic Ventures Co.) The surface oxidation state of porous Pd nanoparticles before and after reactions was detected by x-ray photoelectron spectrometer (Nexsa, Thermo Fisher Scientific) with monochromated, micro-focused, low power Al Kα X-ray source. The possible by-products generated from parallel processes were determined by GC-MS (7890A GC system and 5975C inert MSD, Agilent Technologies).

### Typical photocatalyzed Suzuki–Miyaura reaction condition

In a 1x1 cm quartz cuvette (R-3010-T, Spectrocell), 21 μL bromobenzene (0.2 mmol, 1 equiv.), 36 mg phenylboronic acid (1.5 equiv.), 495 μL CTAC (cetyltrimethylammonium chloride, 400 mM), 600 μL NaOH (sodium hydroxide, 1 M) and 884 μL porous Pd nanoparticles stock solution were added under stirring. The stock porous Pd nanoparticle solution was prepared by dispersing the dry particles in water to have the final ratio of 0.78 % of [Pd<sub>atom</sub>] to [bromobenzene] (0.0078 equiv.) in the reaction solution. Then, the cuvette was sealed by a screw cap with rubber septa, then stirred under 1000 rpm and purged with N<sub>2</sub> for 20 minutes to get rid of oxygen before being irradiated under different LEDs (Mounted type, Thorlabs). The photocatalyzed reactions were under constant stirring at 1000 rpm and controlled at room temperature by using cooling fans. The optical powers before and after the cuvette were recorded by power meters (PM100D console with S170C sensor, Thorlabs) for following calculation of absorbed photon flux. After a certain reaction time, the biphenyl product was extracted from the reaction solution by dichloromethane, then the solvent was evaporated at 50 °C in a vacuum oven for 20 minutes, and the product was dissolved in CDCl<sub>3</sub> and quantified by <sup>1</sup>H-NMR with mesitylene used as the internal standard. The NMR spectra and product yield calculation were listed in Supplementary Note 8.

### Quantum yield calculation

Using the same calculation in our previous work<sup>11</sup>, the quantum yield is defined as the ratio of the number of biphenyl molecules produced per second ( $\Delta N_{biphenyl}/\Delta t$ ) to number of photons absorbed per second ( $N_{abs}/s$ ).

$$Quantum\ Yield\ (\%) = \frac{\#(biphenyl\ produced/s)}{\#(photons\ absorbed/s)} \times 100\ \% = \frac{\frac{\Delta N_{biphenyl}}{\Delta t}}{\frac{N_{abs}}{s}} \times 100\ \%$$

In which:

$$\Delta N_{biphenyl} = 0.2 \text{ mmol} \times \text{Product Yield} \times 6.022 \times 10^{23} \text{ mol}^{-1} \quad (*)$$

$\Delta t$ : reaction time in second

$$\frac{N_{abs}}{s} = \frac{P_{absorbed}}{\frac{hc}{\lambda}} \quad (**)$$

(\*) The product yield of the photocatalyzed reaction was determined by  $^1\text{H-NMR}$  spectroscopy and further corrected by subtracting the background product yield of the non-irradiated reaction within the same reaction time.

(\*\*) ( $N_{abs}/s$ ) were quantified by measuring the optical power at positions before and after the cuvette having the reaction solution during the photoreactions.

$$\text{Photon Flux (photons} \cdot \text{s}^{-1} \cdot \text{cm}^{-2}) = \frac{N_{abs}}{s \times A} = \frac{P_{absorbed}}{\frac{hc}{\lambda} \times \pi(\frac{\varphi}{2})^2}$$

In which:  $\varphi$  is the beam size of the LED light that passes through the cuvette having the reaction solution. The beam size was 0.95 cm, which is smaller than the 1cm width of the cuvette.

## Author Information

### Corresponding author

**Son C. Nguyen** – Department of Chemistry and Chemical Biology, University of California Merced, 5200 North Lake Road, Merced, California 95343, United States; ORCID: 0000-0001-7713-4195; Email: [son@ucmerced.edu](mailto:son@ucmerced.edu)

### Authors

**Pin Lyu** – Department of Chemistry and Chemical Biology, University of California Merced, 5200 North Lake Road, Merced, California 95343, United States; ORCID: 0000-0002-7713-7633

**Randy Espinoza** – Department of Chemistry and Chemical Biology, University of California Merced, 5200 North Lake Road, Merced, California 95343, United States; ORCID: 0000-0002-2825-6724

**Md. Imran Khan** – Department of Physics, University of California Merced, 5200 North Lake Road, Merced, California 95344, United States; ORCID: 0000-0002-5219-0681

**William C. Spaller** – Department of Chemistry and Chemical Biology, University of California Merced, 5200 North Lake Road, Merced, California 95343, United States; ORCID: 0000-0002-1268-9648

**Sayantani Ghosh** – Department of Physics, University of California Merced, 5200 North Lake Road, Merced, California 95344, United States; ORCID: 0000-0003-3440-7194

### Competing interests

The authors declare no competing interests.

### Author contributions

S.C.N and S.G. jointly supervised this work. P.L. designed and carried out the experiments. R.E. synthesized the non-porous Pd nanoparticles. M.I.K. measured the light scattering of the drop-cast mesoporous Pd nanoparticles. W.C.S helped with the organic reactions and revision of manuscript. All authors discussed the results and prepared the manuscript.

## Acknowledgements

The authors would like to thank Duy Nguyen for her fruitful discussions, Anne Pham from the Molecular Foundry of the Lawrence Berkeley National Laboratory and Professor Jennifer Lu from UC Merced for providing technical support for TGA measurements, Professor Peggy A. O'Day for nitrogen gas sorption measurements, and Dr. Liying Zhao from UC Merced for ICP-OES measurements. R. E. acknowledges the research fellowship from Merced Nanomaterials Center for Energy and Sensing (funded by NASA grant no. NNX15AQ01A).

## Data Availability

All relevant data sets supporting this study are available within the article, supplementary information, and source data. Additional data sets are available from the authors depending on the specific aspects by contribution upon reasonable request.

## Reference

- 1 Aslam, U., Rao, V. G., Chavez, S. & Linic, S. Catalytic Conversion of Solar to Chemical Energy on Plasmonic Metal Nanostructures. *Nat. Catal.* **1**, 656-665, doi:10.1038/s41929-018-0138-x (2018).
- 2 Zhou, L. A. *et al.* Quantifying Hot Carrier and Thermal Contributions in Plasmonic Photocatalysis. *Science* **362**, 69-72, doi:10.1126/science.aat6967 (2018).
- 3 Seemala, B. *et al.* Plasmon-Mediated Catalytic O<sub>2</sub> Dissociation on Ag Nanostructures: Hot Electrons or Near Fields? *ACS Energy Lett.* **4**, 1803-1809, doi:10.1021/acseenergylett.9b00990 (2019).
- 4 Chang, L. *et al.* Electronic Structure of the Plasmons in Metal Nanocrystals: Fundamental Limitations for the Energy Efficiency of Hot Electron Generation. *ACS Energy Lett.* **4**, 2552-2568, doi:10.1021/acseenergylett.9b01617 (2019).
- 5 DuChene, J. S., Tagliabue, G., Welch, A. J., Cheng, W. H. & Atwater, H. A. Hot Hole Collection and Photoelectrochemical CO<sub>2</sub> Reduction with Plasmonic Au/p-GaN Photocathodes. *Nano Lett.* **18**, 2545-2550, doi:10.1021/acs.nanolett.8b00241 (2018).
- 6 Kim, Y., Smith, J. G. & Jain, P. K. Harvesting Multiple Electron-Hole Pairs Generated through Plasmonic Excitation of Au Nanoparticles. *Nat. Chem.* **10**, 763-769, doi:10.1038/s41557-018-0054-3 (2018).
- 7 Huang, Y. M. *et al.* Visible Light-Driven Selective Hydrogenation of Unsaturated Aromatics in an Aqueous Solution by Direct Photocatalysis of Au Nanoparticles. *Catal. Sci. Technol.* **8**, 726-734, doi:10.1039/c7cy02291c (2018).
- 8 Kazuma, E. & Kim, Y. Mechanistic Studies of Plasmon Chemistry on Metal Catalysts. *Angew. Chem. Int. Ed.* **58**, 4800-4808, doi:10.1002/anie.201811234 (2019).
- 9 Zhang, Z. L., Zhang, C. Y., Zheng, H. R. & Xu, H. X. Plasmon-Driven Catalysis on Molecules and Nanomaterials. *Acc. Chem. Res.* **52**, 2506-2515, doi:10.1021/acs.accounts.9b00224 (2019).
- 10 Zhao, J. *et al.* A Comparison of Photocatalytic Activities of Gold Nanoparticles Following Plasmonic and Interband Excitation and a Strategy for Harnessing Interband Hot Carriers for Solution Phase Photocatalysis. *ACS Cent. Sci.* **3**, 482-488, doi:10.1021/acscentsci.7b00122 (2017).
- 11 Mao, Z. *et al.* Carrier Diffusion—The Main Contribution to Size-Dependent Photocatalytic Activity of Colloidal Gold Nanoparticles. *ACS Catal.* **9**, 4211-4217, doi:10.1021/acscatal.9b00390 (2019).
- 12 Kim, Y., Dumett Torres, D. & Jain, P. K. Activation Energies of Plasmonic Catalysts. *Nano Lett.* **16**, 3399-3407, doi:10.1021/acs.nanolett.6b01373 (2016).
- 13 Al-Zubeidi, A. *et al.* Hot Holes Assist Plasmonic Nanoelectrode Dissolution. *Nano Lett.* **19**, 1301-1306, doi:10.1021/acs.nanolett.8b04894 (2019).

- 14 Christopher, P. & Moskovits, M. Hot Charge Carrier Transmission from Plasmonic Nanostructures. *Annu. Rev. Phys. Chem.* **68**, 379-398, doi:10.1146/annurev-physchem-052516-044948 (2017).
- 15 Gellé, A. *et al.* Applications of Plasmon-Enhanced Nanocatalysis to Organic Transformations. *Chem. Rev.* **120**, 986-1041, doi:10.1021/acs.chemrev.9b00187 (2020).
- 16 Yu, Y., Wijesekara, K. D., Xi, X. & Willets, K. A. Quantifying Wavelength-Dependent Plasmonic Hot Carrier Energy Distributions at Metal/Semiconductor Interfaces. *ACS Nano* **13**, 3629-3637, doi:10.1021/acsnano.9b00219 (2019).
- 17 Zhang, Y. *et al.* Surface-Plasmon-Driven Hot Electron Photochemistry. *Chem. Rev.* **118**, 2927-2954, doi:10.1021/acs.chemrev.7b00430 (2018).
- 18 Linic, S., Christopher, P. & Ingram, D. B. Plasmonic-Metal Nanostructures for Efficient Conversion of Solar to Chemical Energy. *Nat. Mater.* **10**, 911-921, doi:10.1038/nmat3151 (2011).
- 19 Hou, W. & Cronin, S. B. A Review of Surface Plasmon Resonance-Enhanced Photocatalysis. *Adv. Funct. Mater.* **23**, 1612-1619, doi:10.1002/adfm.201202148 (2013).
- 20 Xin, H., Namgung, B. & Lee, L. P. Nanoplasmonic Optical Antennas for Life sciences and Medicine. *Nat. Rev. Mater.* **3**, 228-243, doi:10.1038/s41578-018-0033-8 (2018).
- 21 Brus, L. Noble Metal Nanocrystals: Plasmon Electron Transfer Photochemistry and Single-Molecule Raman Spectroscopy. *Acc. Chem. Res.* **41**, 1742-1749, doi:10.1021/ar800121r (2008).
- 22 Hou, W. *et al.* Photocatalytic Conversion of CO<sub>2</sub> to Hydrocarbon Fuels via Plasmon-Enhanced Absorption and Metallic Interband Transitions. *ACS. Catal.* **1**, 929-936, doi:10.1021/cs2001434 (2011).
- 23 Liu, L. *et al.* Gold Photosensitized SrTiO<sub>3</sub> for Visible-Light Water Oxidation Induced by Au Interband Transitions. *J. Mater. Chem. A* **2**, 9875-9882, doi:10.1039/C4TA01988A (2014).
- 24 Sundararaman, R., Narang, P., Jermyn, A. S., Goddard Iii, W. A. & Atwater, H. A. Theoretical Predictions for Hot-Carrier Generation from Surface Plasmon Decay. *Nat. Commun.* **5**, 5788, doi:10.1038/ncomms6788 (2014).
- 25 Bernardi, M., Mustafa, J., Neaton, J. B. & Louie, S. G. Theory and Computation of Hot Carriers Generated by Surface Plasmon Polaritons in Noble Metals. *Nat. Commun.* **6**, 7044, doi:10.1038/ncomms8044 (2015).
- 26 Khurgin, J. B. Fundamental Limits of Hot Carrier Injection from Metal in Nanoplasmonics. *Nanophotonics* **9**, 453-471, doi:doi:10.1515/nanoph-2019-0396 (2020).
- 27 Kontoleta, E. *et al.* Using Hot Electrons and Hot Holes for Simultaneous Cocatalyst Deposition on Plasmonic Nanostructures. *ACS. Appl. Mater. Inter.* **12**, 35986-35994, doi:10.1021/acsmi.0c04941 (2020).
- 28 Boltersdorf, J. *et al.* Visible Light-Promoted Plasmon Resonance to Induce “Hot” Hole Transfer and Photothermal Conversion for Catalytic Oxidation. *J. Phys. Chem. C* **122**, 28934-28948, doi:10.1021/acs.jpcc.8b09248 (2018).
- 29 Zhang, C., Jia, F., Li, Z., Huang, X. & Lu, G. Plasmon-generated Hot Holes for Chemical Reactions. *Nano Res.* **13**, 3183-3197, doi:10.1007/s12274-020-3031-2 (2020).
- 30 Zhu, H. *et al.* Mechanism of Supported Gold Nanoparticles as Photocatalysts under Ultraviolet and Visible Light Irradiation. *Chem. Commun.*, 7524-7526, doi:10.1039/B917052A (2009).
- 31 Christopher, P., Xin, H. & Linic, S. Visible-Light-Enhanced Catalytic Oxidation Reactions on Plasmonic Silver Nanostructures. *Nat. Chem.* **3**, 467-472, doi:10.1038/nchem.1032 (2011).
- 32 Mukherjee, S. *et al.* Hot Electrons Do the Impossible: Plasmon-Induced Dissociation of H<sub>2</sub> on Au. *Nano Lett.* **13**, 240-247, doi:10.1021/nl303940z (2013).
- 33 Sakamoto, H. *et al.* Hot-Electron-Induced Highly Efficient O<sub>2</sub> Activation by Pt Nanoparticles Supported on Ta<sub>2</sub>O<sub>5</sub> Driven by Visible Light. *J. Am. Chem. Soc.* **137**, 9324-9332, doi:10.1021/jacs.5b04062 (2015).
- 34 Guerrisi, M., Rosei, R. & Winsemius, P. Splitting of the Interband Absorption Edge in Au. *Phys. Rev. B* **12**, 557-563, doi:10.1103/PhysRevB.12.557 (1975).
- 35 Langhammer, C., Yuan, Z., Zorić, I. & Kasemo, B. Plasmonic Properties of Supported Pt and Pd Nanostructures. *Nano Lett.* **6**, 833-838, doi:10.1021/nl060219x (2006).

- 36 Niu, W. *et al.* Seed-Mediated Growth of Nearly Monodisperse Palladium Nanocubes with Controllable Sizes. *Cryst. Growth Des.* **8**, 4440-4444, doi:10.1021/cg8002433 (2008).
- 37 Molnár, Á. Efficient, Selective, and Recyclable Palladium Catalysts in Carbon–Carbon Coupling Reactions. *Chem. Rev.* **111**, 2251-2320, doi:10.1021/cr100355b (2011).
- 38 Xiao, Q. *et al.* Efficient Photocatalytic Suzuki Cross-Coupling Reactions on Au–Pd Alloy Nanoparticles under Visible Light Irradiation. *Green Chem.* **16**, 4272-4285, doi:10.1039/C4GC00588K (2014).
- 39 Zhang, S. *et al.* Visible-Light-Activated Suzuki–Miyaura Coupling Reactions of Aryl Chlorides over the Multifunctional Pd/Au/Porous Nanorods of CeO<sub>2</sub> Catalysts. *ACS. Catal.* **5**, 6481-6488, doi:10.1021/acscatal.5b01173 (2015).
- 40 Trinh, T. T. *et al.* Visible to Near-infrared Plasmon-enhanced Catalytic Activity of Pd Hexagonal Nanoplates for the Suzuki Coupling Reaction. *Nanoscale* **7**, 12435-12444, doi:10.1039/C5NR03841C (2015).
- 41 Han, D. *et al.* Fabrication of Plasmonic Au–Pd Alloy Nanoparticles for Photocatalytic Suzuki–Miyaura Reactions under Ambient Conditions. *Nanoscale* **9**, 6026-6032, doi:10.1039/C7NR01950E (2017).
- 42 Li, C. *et al.* Pore-Tuning to Boost the Electrocatalytic Activity of Polymeric Micelle-Templated Mesoporous Pd Nanoparticles. *Chem. Sci.* **10**, 4054-4061, doi:10.1039/C8SC03911A (2019).
- 43 Creighton, J. A. & Eadon, D. G. Ultraviolet–Visible Absorption Spectra of the Colloidal Metallic Elements. *J. Chem. Soc., Faraday Trans.* **87**, 3881-3891, doi:10.1039/FT9918703881 (1991).
- 44 Lv, H. *et al.* Mesoporous Gold Nanospheres via Thiolate–Au(i) Intermediates. *Chem. Sci.* **10**, 6423-6430, doi:10.1039/C9SC01728C (2019).
- 45 Lu, Z. *et al.* Porous Pt Nanospheres Incorporated with GO<sub>x</sub> to Enable Synergistic Oxygen-Inductive Starvation/Electrodynamic Tumor Therapy. *Adv. Sci.* **7**, 2001223, doi:10.1002/adv.202001223 (2020).
- 46 Liu, K. *et al.* Porous Au–Ag Nanospheres with High-Density and Highly Accessible Hotspots for SERS Analysis. *Nano Lett.* **16**, 3675-3681, doi:10.1021/acs.nanolett.6b00868 (2016).
- 47 Wang, F. *et al.* Plasmonic Harvesting of Light Energy for Suzuki Coupling Reactions. *J. Am. Chem. Soc.* **135**, 5588-5601, doi:10.1021/ja310501y (2013).
- 48 Sarina, S. *et al.* Viable Photocatalysts under Solar-Spectrum Irradiation: Nonplasmonic Metal Nanoparticles. *Angew. Chem. Int. Ed.* **53**, 2935-2940, doi:https://doi.org/10.1002/anie.201308145 (2014).
- 49 Raza, F. *et al.* Structuring Pd Nanoparticles on 2H-WS<sub>2</sub> Nanosheets Induces Excellent Photocatalytic Activity for Cross-Coupling Reactions under Visible Light. *J. Am. Chem. Soc.* **139**, 14767-14774, doi:10.1021/jacs.7b08619 (2017).
- 50 Biffis, A., Centomo, P., Del Zotto, A. & Zecca, M. Pd Metal Catalysts for Cross-Couplings and Related Reactions in the 21st Century: A Critical Review. *Chem. Rev.* **118**, 2249-2295, doi:10.1021/acs.chemrev.7b00443 (2018).
- 51 Sun, B., Ning, L. & Zeng, H. C. Confirmation of Suzuki–Miyaura Cross-Coupling Reaction Mechanism through Synthetic Architecture of Nanocatalysts. *J. Am. Chem. Soc.* **142**, 13823-13832, doi:10.1021/jacs.0c04804 (2020).
- 52 Nguyen, S. C. *et al.* Study of Heat Transfer Dynamics from Gold Nanorods to the Environment via Time-Resolved Infrared Spectroscopy. *ACS Nano* **10**, 2144-2151, doi:10.1021/acsnano.5b06623 (2016).
- 53 Mao, Z. *et al.* Tuning Redox Potential of Gold Nanoparticle Photocatalysts by Light. *ACS Nano* **14**, 7038-7045, doi:10.1021/acsnano.0c01704 (2020).
- 54 Minutella, E., Schulz, F. & Lange, H. Excitation-Dependence of Plasmon-Induced Hot Electrons in Gold Nanoparticles. *J. Phys. Chem. Lett.* **8**, 4925-4929, doi:10.1021/acs.jpcl.7b02043 (2017).
- 55 Link, S. & El-Sayed, M. A. Shape and Size Dependence of Radiative, Non-radiative and Photothermal Properties of Gold Nanocrystals. *Int. Rev. Phys. Chem.* **19**, 409-453, doi:10.1080/01442350050034180 (2000).

- 56 Un, I.-W. & Sivan, Y. The Role of Heat Generation and Fluid Flow in Plasmon-Enhanced Reduction–Oxidation Reactions. *ACS Photonics*, doi:10.1021/acsp Photonics.1c00113 (2021).
- 57 Kozuch, S. & Martin, J. M. L. “Turning Over” Definitions in Catalytic Cycles. *ACS Catal.* **2**, 2787-2794, doi:10.1021/cs3005264 (2012).
- 58 Lente, G. Comment on “‘Turning Over’ Definitions in Catalytic Cycles”. *ACS Catal.* **3**, 381-382, doi:10.1021/cs300846b (2013).
- 59 Costa, P., Sandrin, D. & Scaiano, J. C. Real-Time Fluorescence Imaging of a Heterogeneously Catalysed Suzuki–Miyaura Reaction. *Nat. Catal.* **3**, 427-437, doi:10.1038/s41929-020-0442-0 (2020).
- 60 Phan, N. T. S., Van Der Sluys, M. & Jones, C. W. On the Nature of the Active Species in Palladium Catalyzed Mizoroki–Heck and Suzuki–Miyaura Couplings–Homogeneous or Heterogeneous Catalysis, A Critical Review. *Adv. Synth. Catal.* **348**, 609-679, doi:10.1002/adsc.200505473 (2006).
- 61 Cong, H. & Porco, J. A. Chemical Synthesis of Complex Molecules Using Nanoparticle Catalysis. *ACS Catal.* **2**, 65-70, doi:10.1021/cs200495s (2012).
- 62 Weaver, J. H. & Benbow, R. L. Low-energy Interband Absorption in Pd. *Phys. Rev. B* **12**, 3509-3510, doi:10.1103/PhysRevB.12.3509 (1975).
- 63 Reiss, H. The Fermi Level and the Redox Potential. *J. Phys. Chem.* **89**, 3783-3791, doi:10.1021/j100264a005 (1985).
- 64 Waidhas, F. *et al.* Secondary Alcohols as Rechargeable Electrofuels: Electrooxidation of Isopropyl Alcohol at Pt Electrodes. *ACS Catal.* **10**, 6831-6842, doi:10.1021/acscatal.0c00818 (2020).
- 65 Bratsch, S. G. Standard Electrode Potentials and Temperature Coefficients in Water at 298.15 K. *J. Phys. Chem. Ref. Data* **18**, 1-21, doi:10.1063/1.555839 (1989).
- 66 Adamo, C., Amatore, C., Ciofini, I., Jutand, A. & Lakmini, H. Mechanism of the Palladium-Catalyzed Homocoupling of Arylboronic Acids: Key Involvement of a Palladium Peroxo Complex. *J. Am. Chem. Soc.* **128**, 6829-6836, doi:10.1021/ja0569959 (2006).
- 67 Pérez-Lorenzo, M. Palladium Nanoparticles as Efficient Catalysts for Suzuki Cross-Coupling Reactions. *J. Phys. Chem. Lett.* **3**, 167-174, doi:10.1021/jz2013984 (2012).
- 68 Wang, F. *et al.* Porous Single-Crystalline Palladium Nanoparticles with High Catalytic Activities. *Angew. Chem. Int. Ed.* **51**, 4872-4876, doi:10.1002/anie.201107376 (2012).
- 69 Huang, S.-C. *et al.* Probing Nanoscale Spatial Distribution of Plasmonically Excited Hot Carriers. *Nat. Commun.* **11**, 4211, doi:10.1038/s41467-020-18016-4 (2020).
- 70 Tagliabue, G. *et al.* Ultrafast Hot-hole Injection Modifies Hot-electron Dynamics in Au/p-GaN Heterostructures. *Nat. Mater.* **19**, 1312-1318, doi:10.1038/s41563-020-0737-1 (2020).
- 71 Tagliabue, G. *et al.* Quantifying the Role of Surface Plasmon Excitation and Hot Carrier Transport in Plasmonic Devices. *Nat. Commun.* **9**, 3394, doi:10.1038/s41467-018-05968-x (2018).

For Table of Contents Only

